SUPPLEMENTAL INFORMATION

Intracellular trafficking of the $K_V1.3$ potassium channel is regulated by the pro-domain of a matrix metalloprotease

Hai M. Nguyen[1*], Charles A. Galea[2*], Galina Schmunk[1], Brian J. Smith[3], Robert A. Edwards[4], Raymond S. Norton[2] and K. George Chandy[1]

[1]Departments of Physiology and Biophysics, and [4]Pathology, School of Medicine, University of California, Irvine, California
[2]Medicinal Chemistry, Monash Institute of Pharmaceutical Sciences, Monash University, Parkville, Victoria 3052, Australia
[3]Department of Chemistry, La Trobe Institute for Molecular Science, La Trobe University, Melbourne, Victoria 3086, Australia

Running Title: MMP23 regulation of potassium channels

To whom correspondence should be addressed:
1. Professor K. George Chandy, Dept. of Physiology and Biophysics, 291 Irvine Hall, School of Medicine, University of California Irvine, Irvine, CA 92697. Fax: 949 8243143; E-mail: gchandy@uci.edu
2. Professor Ray Norton, Medicinal Chemistry, Monash Institute of Pharmaceutical Sciences, Monash University, Parkville, Victoria 3052, Australia. Fax: +61 3 99039167; Email: ray.norton@monash.edu

Table S1. Average R_1, R_2 and R_1/R_2 values for MMP23-PD.

Region	R_1 (s^{-1})	R_2 (s^{-1})	R_1/R_2
MMP23-PD	1.16 ± 0.03	10.79 ± 0.03	0.21 ± 0.02
Transmembrane domain, α1 (residues 16-40)	0.95 ± 0.04	17.71 ± 0.05	0.06 ± 0.01
C-terminal helix (α2; residues 45-60)	1.16 ± 0.02	11.59 ± 0.03	0.11 ± 0.01

Longitudinal (R_1) and transverse (R_2) ^{15}N relaxation rates were obtained at 600 MHz and 30°C for a solution containing 0.7 mM ^{15}N-labelled MMP23-PD in 20 mM sodium citrate (pH 5.0), 100 mM DPC, 20 mM TCEP, 0.02% (w/v) sodium azide, 95% H_2O and 10% ^2H_2O.

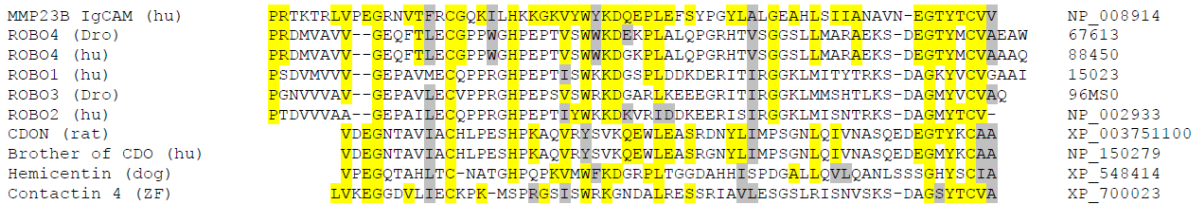

Supplemental Figure S1. Sequence alignment of the IgCAM domain of MMP23's with ROBO proteins. The C-terminal IgCAM domain of MMP23 exhibits high sequence similarity with the ROBO, CDON and brother of CDO proteins. Identical residues are highlighted in yellow, and conserved residues are highlighted in grey.

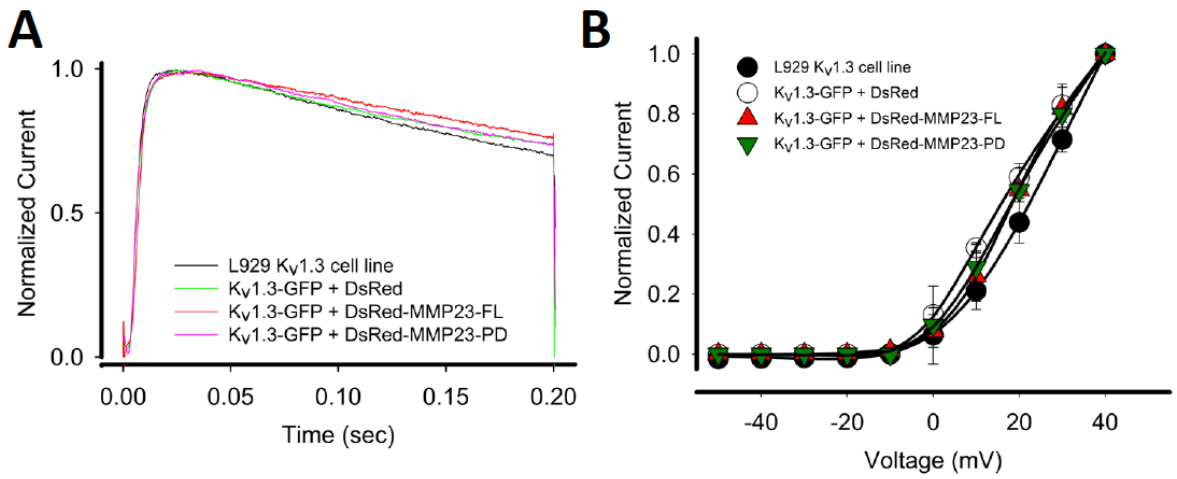

Supplemental Figure S2. Biophysical properties of $K_V1.3$ in cells expressing MMP23-FL or MMP23-PD versus normal $K_V1.3$. *A*, averaged current traces elicited by a +40 mV depolarizing pulse for 200 msec during whole-cell patch-clamping recordings. The activation and inactivation of $K_V1.3$-GFP were the same in cells co-expressing DsRed-MMP23-FL, DsRed-MMP23-PD or the DsRed vector. GFP-tagged $K_V1.3$ channels showed no differences compared to those of untagged $K_V1.3$ stably expressed in the L929 cell line (1). *B*, Current-Voltage relationship of $K_V1.3$ was the same in cells co-expressing DsRed-MMP23-FL, DsRed-MMP23-PD or the DsRed vector.

```
Rat MMP23-PD1       MGWRACLRPEASGA-VQGRWLGAVLSGLCLLSALAFLEWLGSPTETAWNAAQGNVDAPDV  59
Mouse MMP23-PD 1    MGCRACLRPEASGA-VQGRWLGAALSGLCLLSALALLEWLGAPTETAWRAAQGNVDAPNV  59
Human MMP23-PD 1    MGRGARVPSEAPGAGVERRWLGAALVALCLLPALVLLARLGAPAVPAWSAAQGDVAALGL  60


Rat MMP23-PD60       GGSTP-QVPSLLSMLVTRRRRYTLTPARL  87
Mouse MMP23-PD 60    GSSTA-QVPRLLTMSVTRRRRYTLTPARL  87
Human MMP23-PD61     SAVPPTRVPGPLA---PRRRRYTLTPARL  86
```

Supplemental Figure S3. Comparison of sequences of rat, mouse and human MMP23-PD. Rat MMP23 is not processed (cleaved) in mammalian cells despite containing the RRRRY furin cleavage site (6).

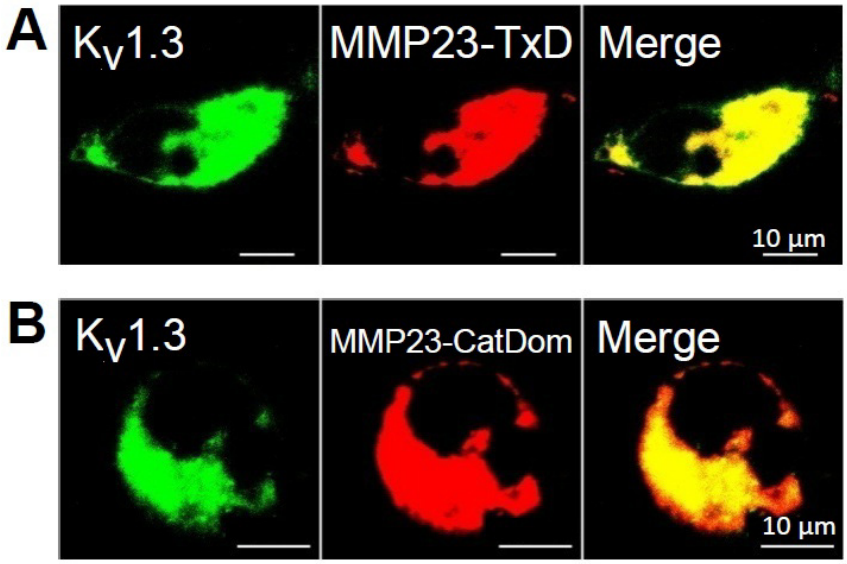

Supplemental Figure S4. Co-localization of MMP23-TxD and MMP23-CatDom with K_V1.3. *A*, confocal images demonstrating that K_V1.3-GFP co-localizes with DsRed-MMP23-TxD. The MMP23-TxD construct contains the pro-domain, the catalytic domain and the TxD. *B*, confocal images demonstrating that K_V1.3-GFP co-localizes with DsRed-MMP23-CatDom. The MMP23-CatDom construct contains the pro-domain and the catalytic domain. The deletion constructs are described in the main text and in Fig. 1, B.

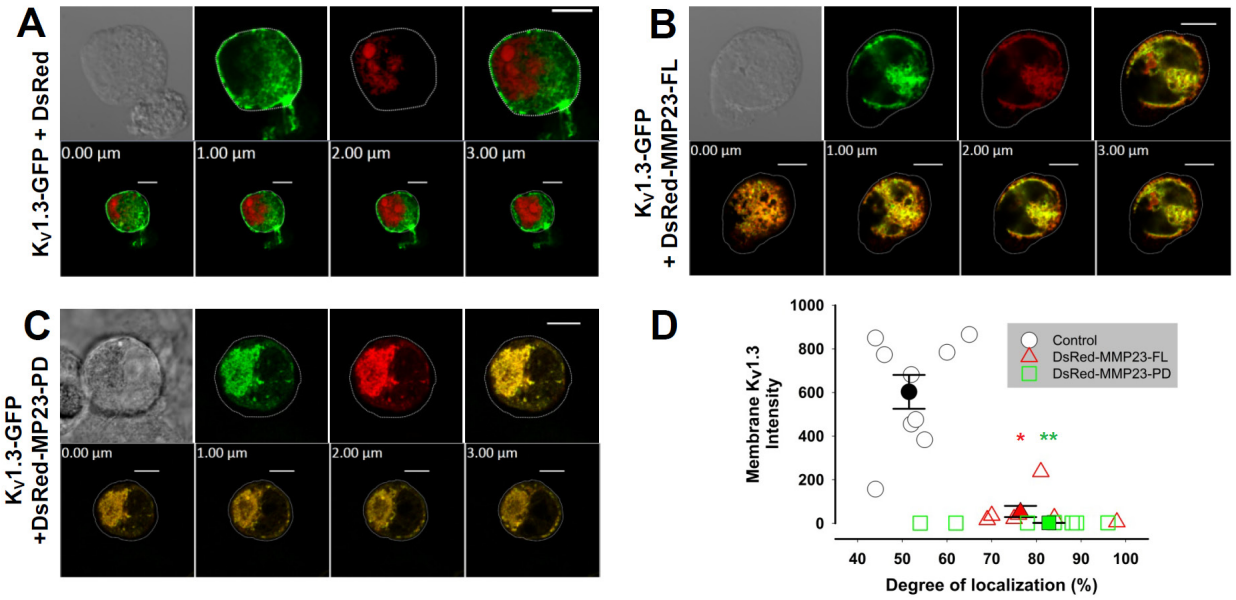

Supplemental Figure S5. Quantification of $K_V1.3$ on the cell surface in cells expressing the DsRed vector versus DsRed-MMP23-FL or DsRed-MMP23-PD. *A,* Confocal images of $K_V1.3$-GFP plus DsRed vector. *B,* $K_V1.3$-GFP plus DsRed-MMP23-FL. *C,* $K_V1.3$-GFP plus DsRed-MMP23-PD. In each top row, the left panel shows a bright-field image, the second panel shows the $K_V1.3$-GFP image, the third panel shows the DsRed image (vector, MMP23-FL, MMP23-PD) and the right panel shows the merged images. *Scale bars* indicate 10 µm in length. Each bottom row shows z-stack images of the respective cell taken at four consecutive planes. *D,* membrane $K_V1.3$ plotted against co-localization index between $K_V1.3$-GFP and dsRed (vector, MMP23-FL, MMP23-PD). Quantification of membrane $K_V1.3$-GFP was calculated from averaged intensity at four different regions of interest (ROI's) at the membrane surface (outlined by dotted-line based on the bright-field image) in each cell. Quantification of co-localization was determined using LSM Zeiss Zen 2011 software (n = 10 cells were imaged for quantification of membrane $K_V1.3$-GFP and co-localization). Statistical significance is determined by *Student's t-test* and indicated by p-values (*, $p < 5x10^{-4}$, **,$p < 1x10^{-4}$)

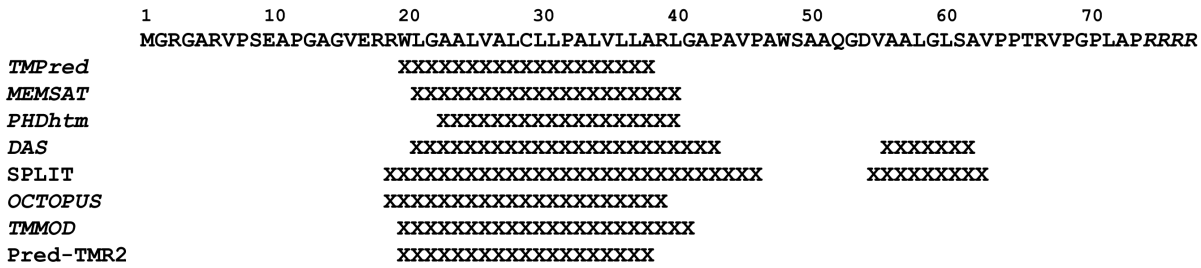

Supplemental Figure S6. MMP23-PD trans-membrane domain (TMD). Predicted TMD for MMP23-PD based on various TMD predictors. "X" denotes residues predicted to lie within a TMD. Predictions of trans-membrane regions were obtained using the following programs: TMPred (2), MEMSTAT (3), PHDhtm (4), DAS (5), Pred-TMR2 (6), SPLIT (7), TMMOD (8), and OCTOPUS (9).

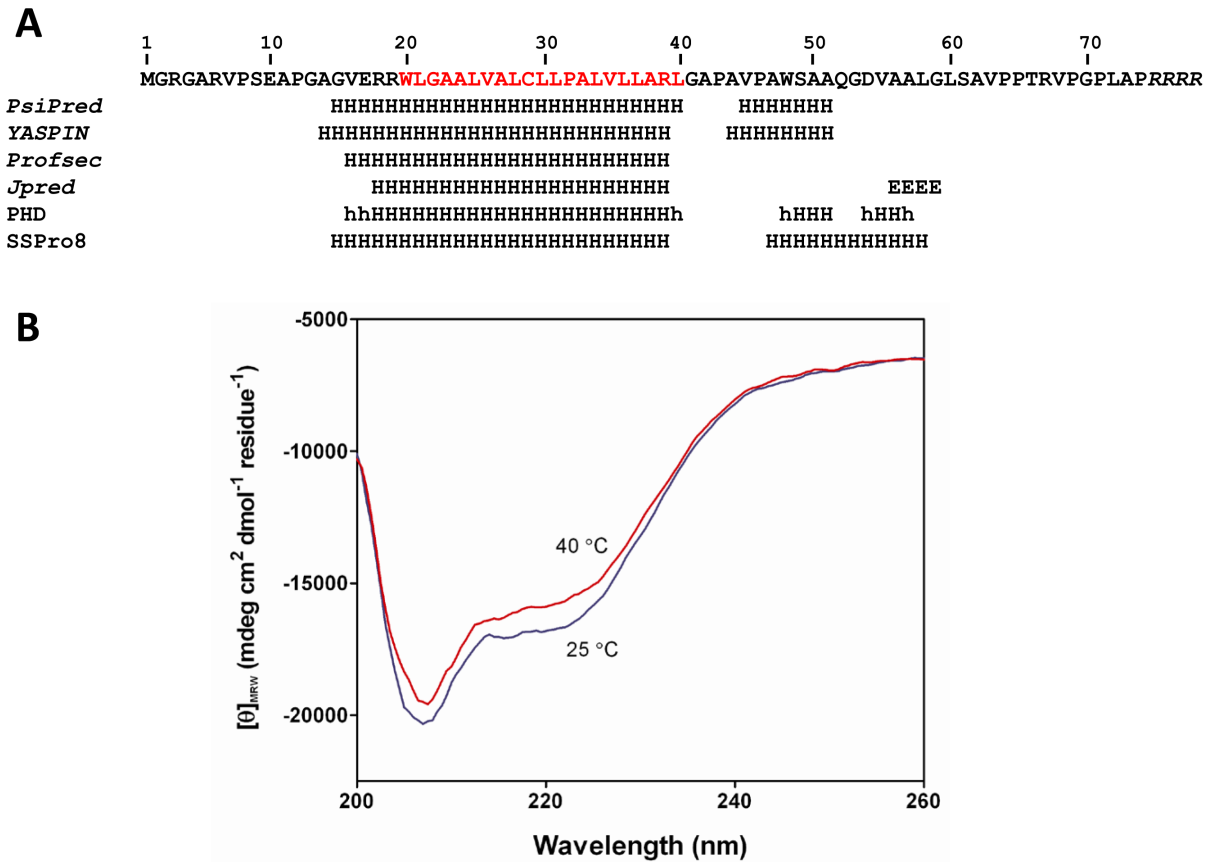

Supplemental Figure S7. Secondary structure of MMP23-PD. *A***,** predicted secondary structure for MMP23-PD using various web-based secondary structure predictors. The predicted TMD is highlighted in red. "H" denotes predicted α-helical regions and "E" β-strand regions. Secondary structure was predicted using the web-based secondary structure prediction programs Jpred (10), PHD (11), YASPIN (12), Profsec (11), PsiPred (13) and SSPro8 (14). *B***,** CD spectral analysis of MMP23-PD in DPC micelles at 25 and 40°C.

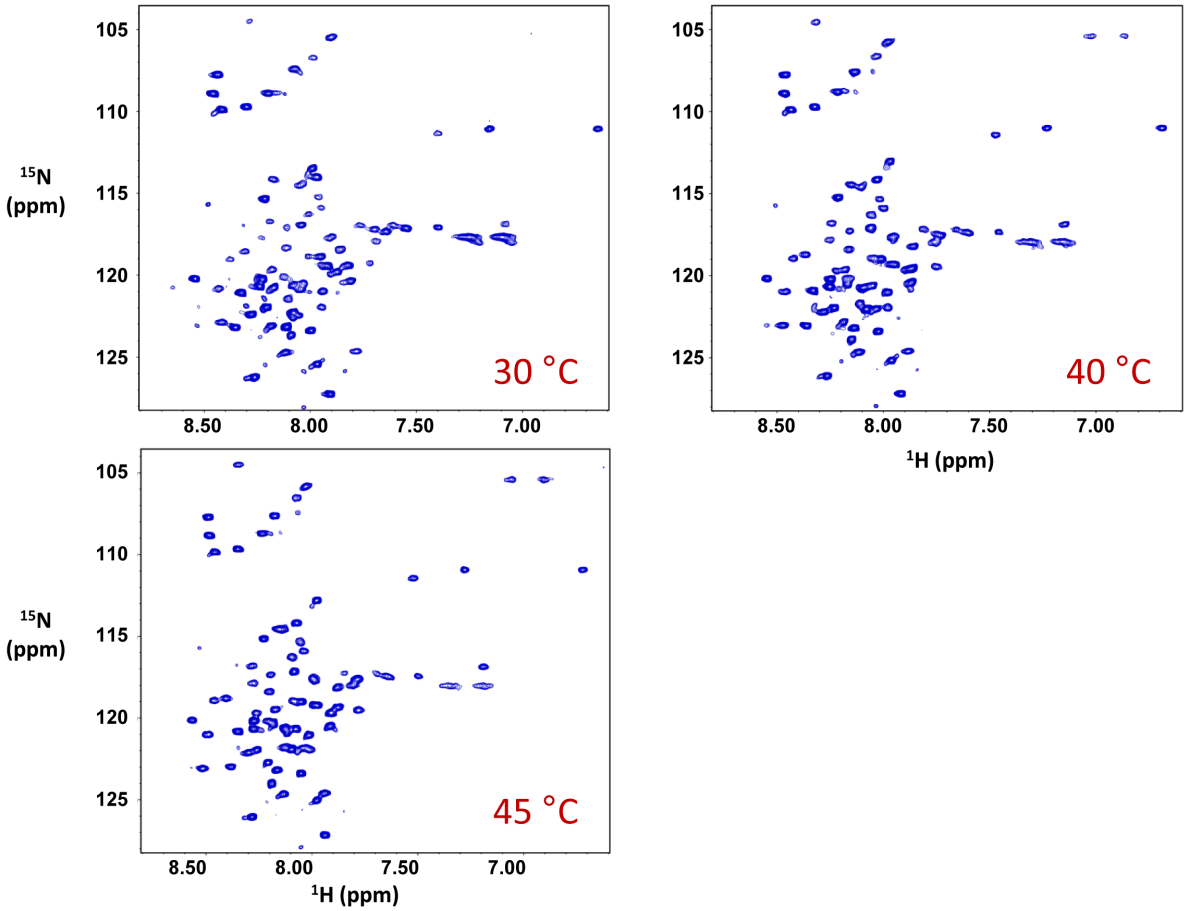

Supplemental Figure S8. HSQC spectra of MMP23-PD at various temperatures. The sample contained 0.7 mM MMP23-PD in 20 mM sodium citrate buffer (pH 5.0), 100 mM DPC, 20 mM TCEP, 0.02% NaN_3 and 10% ^2H_2O. Spectra were acquired on a Varian Inova 600 MHz spectrometer at the indicated temperatures.

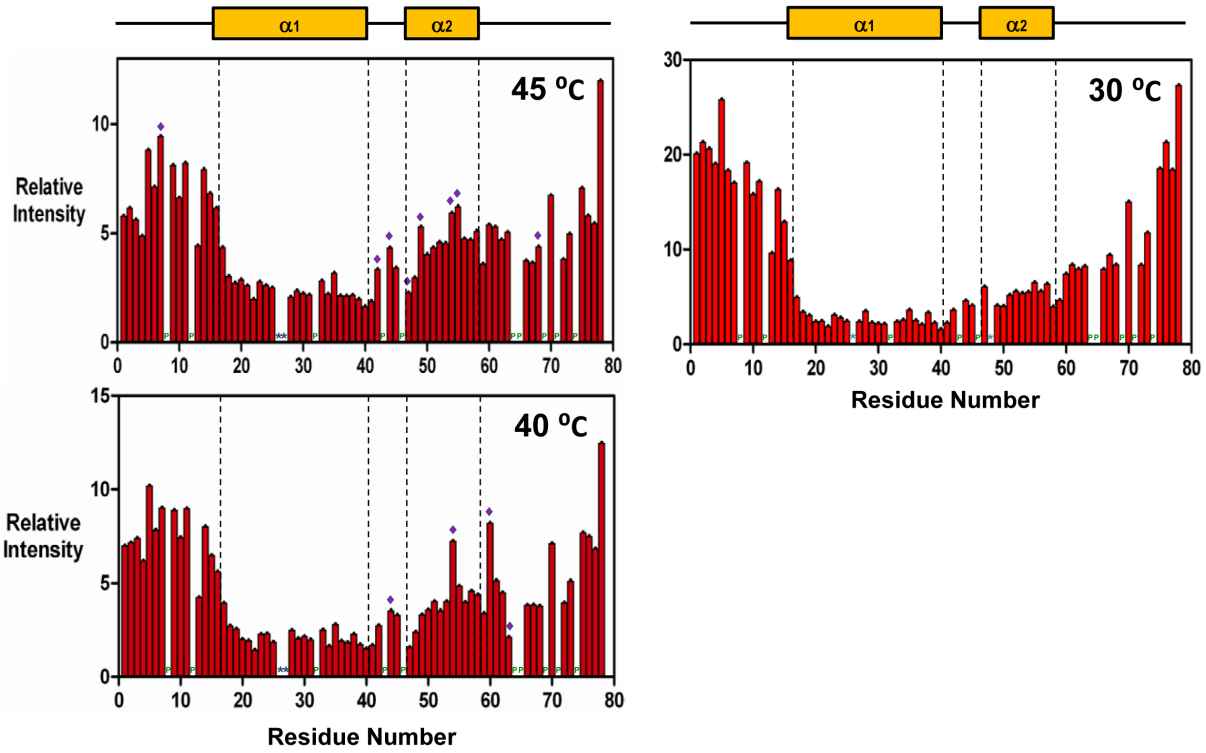

Supplemental Figure S9. Relative cross-peak intensities in [^{1}H-^{15}N] HSQC spectra of MMP23-PD at 30, 40 and 45°C. The secondary structure for MMP23-PD is shown at the top. Overlapped peaks are denoted with a purple diamond. Proline residues are denoted with a "P" and residues for which no data were available an asterisk. Note that cross-peak intensities are more uniform at the higher temperatures.

A

```
                    1         10                  20        30        40          50
Giant Panda (G1m504) MGLGACMSSAA-----SGARAQARRLEAVLGAVCLLPVLLLLPTGWDRKPENAERPKEGD
Dog (E2R4V4)         MGLGACVSSAA-----SGAQAQARWLGAVLGALCLLPVLLLLARPGAPAARLGASAAQGD
Porcine (F1RJC6)     MGRRACVPSAA-----SGARDQARRLGAVLGALCLLPALLLLARLGAPAARLAASAAQGD
Bovine (Q2TBM7)      MGRGACVPSAA-----SGAGDRARQLGAVLGALCLFPALVLLAWPGTPANGAGARVAQGD
Human (O75900)       MGRGARVPSEA-----PGAGVERRWLGAALVALCLLPALVLLARLGAPAVP-AWSAAQGD
Opossum (F7CDE4)     MGPGVNPPAEP-----PGGTARMPSYRALLGLLCLLPALALLLTLKDTADP-EARGSQED
Chicken (E1BX58)     MDQIEQLSADRKKNFLSEDNKKSNGYRTVVGFLCIFPVVALLAIAGDPAGV-AVQESQED
                     *.     .:       .    .     : :  :*::*.: **              : *
```

B

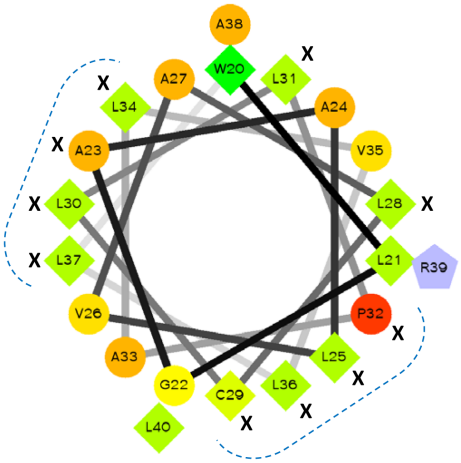

Supplemental Figure S10. Conservation of residues within the TMD of MMP23-PD. *A*, sequence alignment of MMP23-PD from different species, where the predicted TMD is highlighted by an orange box. The sequence alignment was performed using ClustalW (15). Residues that are identical, conserved or semi-conserved across species are denoted by the symbols "*", ":" or ".", respectively. Residues are numbered according to human MMP23-PD. *B*, helical wheel representation generated using the web-based program WHEEL (http://rzlab.ucr.edu/scripts/wheel/wheel.cgi) for residues within the predicted TMD of (human) MMP23-PD. Identical and conserved residues within the MMP23-PD TMD are denoted by "×" and residues that cluster on separate faces of the helical wheel are denoted by a dotted blue line. Residues are represented as follows: hydrophilic - circles, hydrophobic – diamonds and potentially positively charged as pentagons. Residues are color-coded according to hydrophobicity/hydrophilicity, from red (most hydrophilic) through yellow (moderately hydrophilic) to green (most hydrophobic). Potentially charged residues are colored light blue.

REFERENCES

1. Grissmer, S., Nguyen, A. N., Aiyar, J., Hanson, D. C., Mather, R. J., Gutman, G. A., Karmilowicz, M. J., Auperin, D. D., and Chandy, K. G. (1994) Pharmacological characterization of five cloned voltage-gated K^+ channels, types Kv1.1, 1.2, 1.3, 1.5, and 3.1, stably expressed in mammalian cell lines *Mol. Pharmacol.* **45,** 1227-1234
2. Hofmann K and Stoffel W (1993) TMbase - A database of membrane spanning proteins segments *Biol Chem Hoppe-Seyler* **374,** 166
3. Jones, D. T., Taylor, W. R., and Thornton, J. M. (1994) A model recognition approach to the prediction of all-helical membrane protein structure and topology *Biochemistry* **33,** 3038-3049
4. Rost, B., Casadio, R., Fariselli, P., and Sander, C. (1995) Transmembrane helices predicted at 95% accuracy *Protein Sci.* **4,** 521-533
5. Cserzo, M., Wallin, E., Simon, I., von, H. G., and Elofsson, A. (1997) Prediction of transmembrane alpha-helices in prokaryotic membrane proteins: the dense alignment surface method *Protein Eng* **10,** 673-676
6. Pasquier, C. and Hamodrakas, S. J. (1999) An hierarchical artificial neural network system for the classification of transmembrane proteins *Protein Eng* **12,** 631-634
7. Juretic, D., Zoranic, L., and Zucic, D. (2002) Basic charge clusters and predictions of membrane protein topology *J. Chem Inf. Comput. Sci.* **42,** 620-632
8. Kahsay, R. Y., Gao, G., and Liao, L. (2005) An improved hidden Markov model for transmembrane protein detection and topology prediction and its applications to complete genomes *Bioinformatics.* **21,** 1853-1858
9. Viklund, H. and Elofsson, A. (2008) OCTOPUS: improving topology prediction by two-track ANN-based preference scores and an extended topological grammar *Bioinformatics.* **24,** 1662-1668
10. Cole, C., Barber, J., and Barton GJ (2008) The Jpred 3 secondary structure prediction server *Nucleic Acids Res* **36,** 197-201
11. Rost, B., Yachdav, G., and Liu, J. (2004) The PredictProtein server *Nucleic Acids Res.* **32,** W321-W326
12. Lin, K., Simossis, V. A., Taylor, W. R., and Heringa, J. (2005) A simple and fast secondary structure prediction method using hidden neural networks *Bioinformatics.* **21,** 152-159
13. McGuffin, L. J., Bryson, K., and Jones, D. T. (2000) The PSIPRED protein structure prediction server *Bioinformatics.* **16,** 404-405
14. Pollastri, G., Przybylski, D., Rost, B., and Baldi, P. (2002) Improving the prediction of protein secondary structure in three and eight classes using recurrent neural networks and profiles *Proteins* **47,** 228-235
15. Thompson, J. D., Higgins, D. G., and Gibson, T. J. (1994) CLUSTAL W: improving the sensitivity of progressive multiple sequence alignment through sequence weighting, position-specific gap penalties and weight matrix choice *Nucleic Acids Res* **22,** 4673-4680